metals

MDPI

Article

Effect of Oxidation Temperature on the Oxidation Process of Silicon-Containing Steel

Bei He, Guang Xu *, Mingxing Zhou and Qing Yuan

The State Key Laboratory of Refractories and Metallurgy, Hubei Collaborative Innovation Center for Advanced Steels, Wuhan University of Science and Technology, 947 Heping Avenue, Qingshan District, Wuhan 430081, China; 15071412662@163.com (B.H.); kdmingxing@163.com (M.Z.); 15994235997@163.com (Q.Y.)
* Correspondence: xuguang@wust.edu.cn; Tel.: +86-15697180996

Academic Editor: Hugo F. Lopez
Received: 21 April 2016; Accepted: 27 May 2016; Published: 7 June 2016

Abstract: The oxidation behavior of silicon-containing steel was studied by applying segmented heating routes similar to the atmosphere and heating process in an industrial reheating furnace. The oxidation tests were carried out on a simultaneous thermal analyzer at heating temperatures of 1150 °C–1300 °C. The morphologies of Fe_2SiO_4 were observed by SEM, and the penetration depths of the Fe_2SiO_4 layer at different oxidation temperatures were determined by using the Image-Pro Plus 6.0 software. The results show that at heating temperatures ⩾1235 °C, the oxidation rate and total oxidation mass gain have no relation with the heating temperature; the mass gain versus time follows a linear law after about 1164 °C (lower than the eutectic temperature of fayalite). In addition, the oxidation rate first decreases slowly and then drops from 1190 °C to 1210 °C during the isothermal holding stage. With the increase in temperature, the oxidation rate and mass gain also increase gradually; the relationship between the mass gain and time is close to a parabolic law. Moreover, at a heating temperature of 1150 °C, the oxidation rate decreases rapidly during the isothermal holding stage, and the mass gain versus time follows a parabolic law.

Keywords: oxidation temperature; oxide scale; fayalite; oxidation kinetics

1. Introduction

Silicon (Si) is an important alloying element for improving the corrosion resistance and mechanical performance of conventional alloys [1–3]. However, the addition of Si often leads to red scale, a surface defect of hot rolled steels [4]. In Si-containing steels, red scale is related to the presence of fayalite (Fe_2SiO_4) which forms by the combination of SiO_2 and FeO, firmly bonding steel substrate and iron scale [5,6]. The melting point of Fe_2SiO_4 is about 1173 °C and liquid Fe_2SiO_4 irregularly penetrates into FeO and the matrix. It is difficult to completely wipe off the FeO layer after descaling due to the very high strength of the eutectic compound Fe_2SiO_4/FeO. The remaining FeO scale is oxidized into red Fe_2O_3 during following cooling process. The oxidation temperature influences the oxidation process and Fe_2SiO_4 morphology during the reheating process [7–9]. So far, some studies on the effects of the oxidation temperature on the oxidation mass gain and Fe_2SiO_4 have been reported.

Suarez *et al.* [10] found that oxidation treatments in air at temperatures higher than 570 °C lead to three different iron oxide layers: wustite (FeO), magnetite (Fe_3O_4) and hematite (Fe_2O_3), in increasing order of oxygen content, going from substrate to free surface. Below 570 °C, only the last two layers are thermodynamically stable. Cao *et al.* [11] investigated the isothermal oxidation kinetics of low carbon steel at temperatures ranging between 500 °C and 900 °C. They reported that the oxidation mass gain per unit area with time has a parabolic relation and that the oxidation rate decreases with time. Mouayd *et al.* [12] studied the oxidation of silicon-containing steels in the temperature range of 900 °C–1200 °C. They found that a passivation period occurs during the oxidation of silicon steels

and that a high silicon concentration leads to a long passivation of oxidation at temperatures lower than 1173 °C. The passivation period is due to the formation of a thin silica layer as Si is more prone to oxidation than iron. This layer dramatically slows down the diffusion of Fe^{2+} towards the surface in contact with the oxidizing atmosphere. Fukagawa *et al.* [13] and Okada *et al.* [5] reported that when the temperature reaches 1173 °C (the eutectic temperature of fayalite), the liquid FeO/Fe_2SiO_4 flows into the external scale and develops a net-like distribution, considerably increasing the scale thickness of Fe-Si alloy.

In previous studies, the oxidation atmosphere was usually introduced into the chamber of the simultaneous thermal analyzer (STA) during the isothermal oxidation stage. Few studies have adopted heating routes similar to those in the reheating technology used in the industrial production of hot strips; *i.e.*, steel slabs are kept in an oxidation atmosphere at temperatures ranging from low to high temperature during the whole reheating process. In addition, the heating temperatures applied in most studies were below 1200 °C, whereas the heating temperature in industrial production is higher than 1200 °C in most cases. Therefore, it is necessary to investigate the oxidation process of silicon-containing steels under an oxidation atmosphere and temperature similar to those used in industrial production. In the present study, the oxidation kinetics of silicon-containing steel was investigated by using oxidation atmosphere and temperatures similar to those applied in the industrial reheating process. The results provide theoretical reference for controlling oxide scale defects and preventing red scale on the surface of silicon-containing steels.

2. Materials and Methods

Silicon-containing steel composed of Fe-0.07C-1.11Si-1.2Mn-0.035Al-0.016Cr (wt. %) was obtained from a hot strip plant. The oxidation tests were carried out on a Setaram Setsys Evo STA (Setaram, Lyon, France). The dimensions of the samples were 15 mm × 10 mm × 3 mm. A hole with a diameter of 4 mm was drilled near the edge center in each sample for suspension in the oxidation chamber. The surfaces of all samples were polished on a series of SiC polishing paper up to 2000 to remove the scale before the tests. The experimental procedure was designed according to the industrial reheating process, as shown in Figure 1. The samples were first heated to 850 °C at a rate of 20 °C/min and then heated to predetermined temperatures (1150, 1190, 1210, 1235, 1260 and 1300 °C) at a slower heating rate of 6.6 °C/min; they were kept at these temperatures for different periods to ensure the same total heating time for all samples. After the isothermal holding, the samples were cooled to room temperature at a rate of 50 °C/min. The accuracy of temperature measurement is ±0.5 °C, so that the effect of thermal drifts of thermobalance setup on mass gain could be ignored. The atmosphere for slabs in industrial reheating furnace contains 4.0 vol. % oxygen. A binary gas mixture of oxygen and nitrogen with an oxygen concentration of 4.0 vol. % was introduced into the STA chamber during the heating and holding stages to simulate the oxidizing atmosphere of reheating furnace in the industrial production process; the oxygen concentration was changed to 21.0 vol. % during the cooling stage to simulate the oxygen concentration in the air. The mass gain of the samples and the temperature were digitally recorded during the oxidation processes.

After the oxidation tests, the samples were molded in resins at room temperature to protect the integrity of the oxide scale. The cross-sections of mounted samples were ground and polished. The microstructures of the oxide scale were observed on a Nova 400 Nano scanning electron microscope (SEM) (FEI, Hillsboro, OR, USA) operated at an accelerating voltage of 20 kV. In addition, the penetration depths of the Fe_2SiO_4 layer at different oxidation temperatures were determined by using the Image-Pro Plus 6.0 software (Media Cybernetics, Rockville, MD, USA).

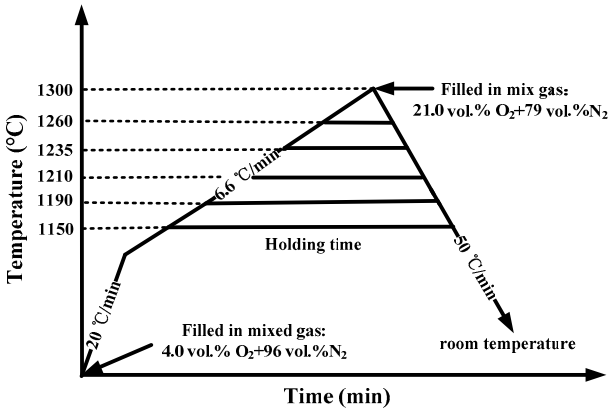

Figure 1. Oxidation experiment route.

3. Results and Discussions

3.1. Morphology of Fe_2SiO_4

Figure 2 shows the morphologic images of Fe_2SiO_4 at different oxidation temperatures. Table 1 presents the main atomic percentages of the inner layer at temperature 1260 °C (Figure 2e); the inner layer is a composite of eutectic compounds Fe_2SiO_4/FeO. The bright area (Spectrum 1) is FeO, while the dark area (Spectrum 2) is mainly Fe_2SiO_4. In addition, Mn is detected in the bright and dark area. The constitution of the inner layer is consistent with the results in the other studies [14,15]. Figure 2 shows that the granular FeO + Fe_2SiO_4 layer is dispersed close to the substrate at 1150 °C. However, a continuous net-like distribution layer of FeO + Fe_2SiO_4 is observed at 1190 to 1300 °C. At temperatures higher than the melting point of Fe_2SiO_4 (1173 °C), the liquid Fe_2SiO_4 is forced to penetrate at the grain boundaries of the steel substrate and oxide scale [16–18]. The penetration depths of Fe_2SiO_4 at different oxidation temperatures were measured by using the Image-Pro Plus 6.0 software (Figure 3). Several images were used to improve the accuracy of Fe_2SiO_4 measurement. With the increase in temperature from 1150 to 1190 °C, the depth of Fe_2SiO_4 increases significantly. However, at temperatures ranging from 1190 to 1235 °C, the depth of Fe_2SiO_4 increases slowly. As the temperature increases further, the depth of Fe_2SiO_4 shows no significant change.

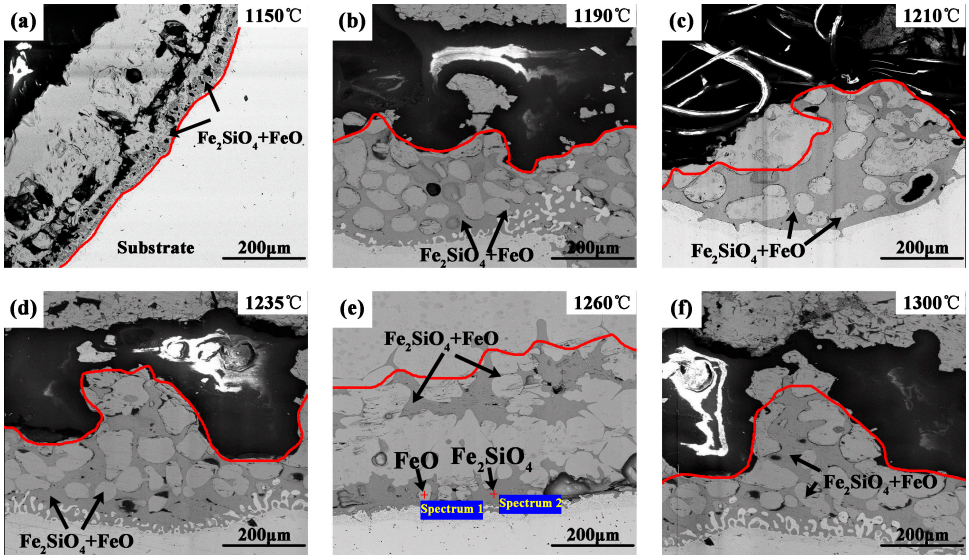

Figure 2. SEM cross-section micrographs showing the distribution of Fe_2SiO_4 at different oxidation temperatures: (**a**) 1150 °C; (**b**) 1190 °C; (**c**) 1210 °C; (**d**) 1235 °C; (**e**) 1260 °C; (**f**) 1300 °C.

Table 1. Main atomic percentages of different layers (at. %).

Chemical Elements	O	Si	Fe	Mn
Bright area (Spectrum 1)	53.71	-	45.62	0.67
Dark area (Spectrum 2)	59.66	12.16	27.29	0.89

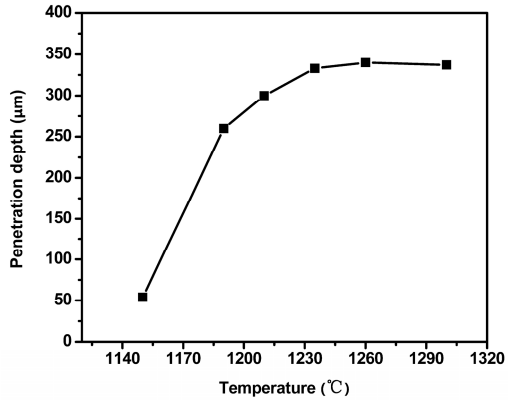

Figure 3. Penetration depths of Fe_2SiO_4.

3.2. Oxidation Analysis

Figure 4 shows the mass gain per surface square centimeter of samples and the oxidation rate as functions of time at different oxidation temperatures. The whole oxidation process includes three stages; slow oxidation, intense oxidation, and final stop oxidation. At a heating temperature ⩾1235 °C, during the intense oxidation stage, the oxidation rate remains constant, and the mass gain per surface unit with time follows a linear law. At temperatures ranging from 1190 to 1235 °C, during the intense oxidation stage, the oxidation rate first decreases slowly and then drops obviously. The mass gain per surface square centimeter with time is close to a parabolic law. At 1150 °C (lower than the eutectic temperature of fayalite-wustite), during the intense oxidation stage, the mass gain versus time shows a parabolic relationship. There are three critical temperatures: the starting oxidation temperature (SOT, point A), the intense oxidation temperature (IOT, point B), and the finishing oxidation temperature (FOT, point C). Before the SOT, the rates of diffusion and combination among ions are slow due to the lower temperature; thus, the sample is almost not oxidized. Between the SOT and the IOT, the adhesion of Si and O_2 is stronger than that of Fe and O_2 at low temperatures [19,20], leading to the appearance of SiO_2 before the formation of the FeO. Because SiO_2 retards the diffusion of iron ions and oxygen atoms, the oxidation reaction is slow as the temperature increases. The jump in oxidation rate is due to a buoyancy effect, caused by turbulent gas flows at about 43 min in Figure 4b. At the intense oxidation temperature, the oxidation rate increases dramatically. This is due to the considerable increase in the diffusion rate at higher temperatures [21–24], resulting in a sharp increase in the oxidation rate. After the FOT, the oxidation reaction stops rapidly. According to the mass grain curves, the three critical temperatures at different oxidation temperatures are determined (Table 2). Because the oxygen concentration increases to 21.0 vol. %, the oxidation rate increases dramatically at the beginning of the cooling process.

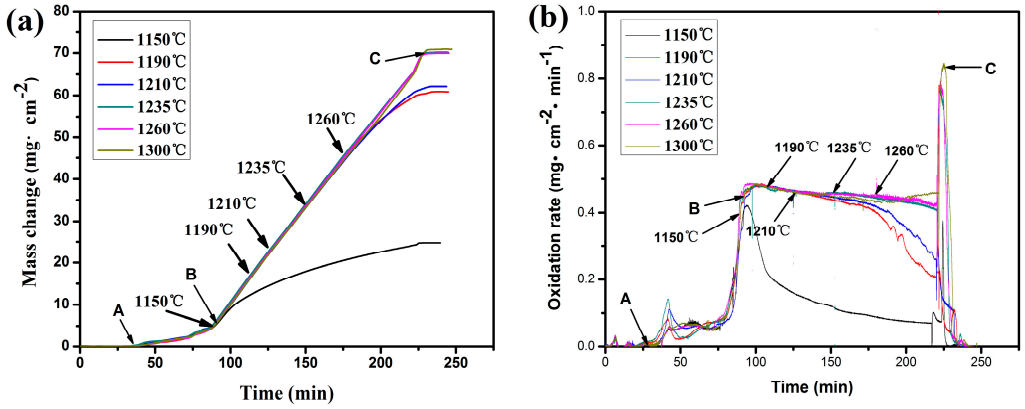

Figure 4. (**a**) Mass gain versus time and (**b**) oxidation rate versus time at 1150 to 1300 °C.

Table 2. Transition temperatures of the oxidation reaction.

Oxidation Temperature/°C	Starting Oxidation Temperature (A)/°C	Intense Oxidation Temperature (B)/°C	Finishing Oxidation Temperature (C)/°C
1150	480	1150	803
1190	483	1161	1158
1210	506	1167	1160
1235	491	1164	1162
1260	487	1162	1161
1300	494	1167	1166

Regarding to the oxidation kinetics at constant heating temperature, it is often reported that the mass gain and heating time follows parabolic rule [12,15]. The results in the present study indicate that the mass gain versus time follows the parabolic law at the temperature below 1210 °C. However, mass gain changes linearly with time at the heating temperature higher than 1235 °C. This point is useful for the determination of heating routes of silicon-containing steels in industrial production of hot strip because the heating temperature is often higher than 1235 °C. The results demonstrate that the total mass gains of oxidation are the same at the temperature above 1235 °C.

The oxidation kinetics during the isothermal holding period at temperatures below 1235 °C can be described by a parabolic formula proposed by Kofstad *et al.* [25]:

$$\Delta W^n = K_p \cdot t \, (n > 1) \tag{1}$$

The oxidation kinetics during the isothermal holding period at temperatures higher than 1235 °C can be represented by a linear equation:

$$\Delta W = K_l \cdot t \tag{2}$$

where, ΔW is the mass gain of the oxide scale in mg/cm^2; K_l and K_p are the oxidation rate constants at a constant temperature T; and t is the oxidation time. The value of n in Equation (1) varies from 1 to 2 from a linear relationship to a parabolic law. Therefore, Equation (2) can be integrated into Equation (1).

The oxidation rate constants for different heating temperatures can be calculated based on the experimental data, as shown in Table 3. The kinetic constants increase at 1150 to 1210 °C but remain similar at temperatures higher than 1235 °C.

As shown in Figure 4 and Table 2, there is no significant change in the intense oxidation temperatures at a heating temperature ⩾1190 °C, and the average IOT is 1164 °C. The IOT is a temperature range of about 1060 °C–1164 °C, where the end of temperature of the interval is selected as IOT in this paper. It is interesting to note that the intense oxidation temperatures are lower than

the eutectic temperature of fayalite (1173 °C), indicating that the intense oxidation has no relationship with the melting of fayalite.

Table 3. Oxidation kinetics parameters.

Temperature (°C)	K_l (mg·cm^{-2}·min^{-1})	K_p (mg^2·cm^{-4}·min^{-1})
1150	-	0.075
1190	-	0.141
1210	-	0.318
1235	0.452	-
1260	0.459	-
1300	0.454	-

At temperatures higher than 1164 °C, during the heating stage, the oxidation rate shows no significant change (Figure 4b). Regarding to the oxidation of steels, five main factors should be considered. Firstly, the radius of the oxygen ion is much larger than that of the iron ion; thus, it is difficult for the oxygen ion to diffuse into the reaction interface [26]. As a result, the oxidation rate depending on the diffusion of iron ions increases with the temperature. The liquid Fe_2SiO_4 provides diffusion passages for diffusion of iron ions. Thus, the mass gain increases with the temperature. Secondly, manganese (Mn) in the steel substrate can be oxidized [6]. Manganese oxides which are detected in Table 1 increase the oxidation mass gain. Thirdly, the oxidation reaction of carbon (C) causes decarburization in the steel. Simultaneous scaling and decarburization has been studied [27,28], and the general consensus is that during steel oxidation, carbon reacts with the scale via the following reaction [28]:

$$[C] + FeO = Fe + CO \quad (3)$$

where [C] denotes carbon in solution in steel. Further reaction between CO and the scale may produce CO_2 via the following reaction:

$$CO + FeO = Fe + CO_2 \quad (4)$$

From the reactions, mass loss due to decarburization overlaps with the mass gain from the oxidation. Fourthly, wustite occurs with a broad composition range that can be described as $Fe_{1-x}O$, with x varying from 0.04 to 0.17 [11]. The ion transport through oxides is dominated by the stoichiometry of the oxide (wustite) that is p-type [26,29]. The fact that x is always positive implies that wustite is cation-deficient and that the interaction between cations and vacancies is the predominant mechanism of mass transport. The amount of iron ions increases and the vacancies of iron ions decrease with the increasing of temperature, leading to a reduction in diffusion passages. Therefore, the oxidation rate decreases with the increase of temperature. Fifthly, the thickness of oxide scale hinders the diffusion of iron ion, decreasing the oxidation rate. The fact that oxidation rate at temperatures higher than 1164 °C has no significant change in Figure 4b indicates the dynamic equilibrium of above five factors affecting oxidation rate. In addition, linear mass gain could be caused by a constant gradient in chemical potential that drives oxygen/iron diffusion.

In addition, as shown in Figure 4, at heating temperatures ranging from 1235 to 1300 °C, the oxidation rates of the samples are basically the same, and the mass gain versus time follows an almost linear relationship, indicating that the oxidation mass gain is not sensitive to temperature. The liquid Fe_2SiO_4 is forced to penetrate at the grain boundaries of the steel substrate and oxide scale, which plays a role as passage for the ions transfer process and provides fast diffusion passages to accelerate the oxidation rate [14]. In the isothermal holding process at 1235 °C, the oxidation rates of Fe, Mn and C can reach dynamic equilibrium during the isothermal holding period. Therefore, the oxidation rate remains constant. At temperatures higher than 1235 °C, the oxidation rates of Fe, Mn and C can reach dynamic equilibrium, resulting in the same oxidation rate. Therefore, the oxidation rate is not sensitive to temperature.

Figure 5a shows the oxidation rate as a function of time in the isothermal holding period at 1150 °C. As indicated in the figure, the oxidation rate decreases rapidly; Figure 4a shows that the mass gain versus time has a parabolic relationship. Because the oxygen concentration is constant, the oxidation reaction is mainly determined by the iron ion concentration in the interface reaction during the isothermal holding period at 1150 °C. The thickness of the oxide scale, the amount of solid-phase particles of SiO_2 and Fe_2SiO_4 increase during the isothermal holding period at 1150 °C, which is unfavorable for ion diffusion. Therefore, the iron ion concentration in the reaction interface decreases quickly, resulting in a rapid decrease in the oxidation rate.

Moreover, as shown in Figure 5b, the oxidation rate first decreases slowly and then reduces obviously during the isothermal holding period at 1190 °C and 1210 °C. In the isothermal holding period, the amount of liquid Fe_2SiO_4 increases with the oxidation time, promoting the diffusion of ions. However, at the same time, the thickness of the oxide scale increases, which is unfavorable for ion diffusion. At the beginning of the isothermal holding period, the promotion and inhibition effect on the ion diffusion of the oxidation reaction basically reach dynamic equilibrium. Therefore, the oxidation rate decreases slowly. With the progress of the isothermal holding time, the thickness of the oxide scale increases such that the inhibition effect on the ion diffusion becomes greater than the promotion effect. Therefore, the oxidation rate decreases obviously with time. In addition, the promotion effect of temperature on the ion diffusion increases with the temperature, resulting in a slightly higher oxidation rate at high heating temperatures. Because Fe_2SiO_4 is in solid phase at 1150 °C, which hinders the diffusion of ions, the decrease in oxidation rate at 1150 °C is significantly greater than that at 1190 °C and 1210 °C during the isothermal holding period.

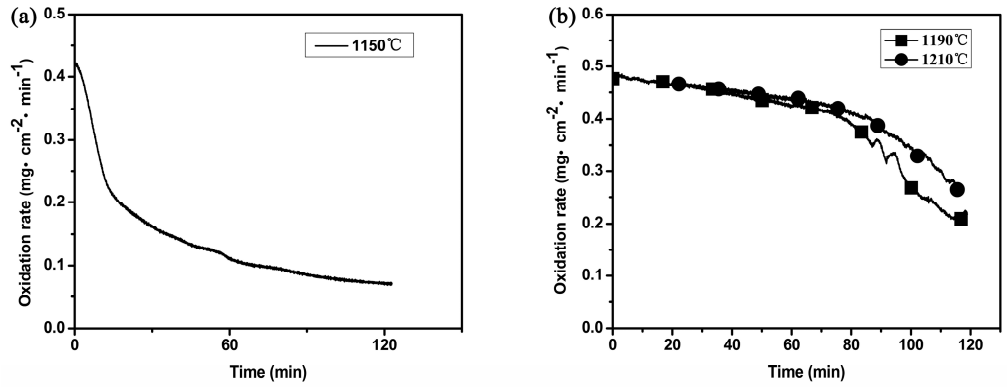

Figure 5. Oxidation rate versus time during the isothermal holding period: (**a**) 1150 °C; (**b**) 1190 °C and 1210 °C.

Figure 6 presents the total mass gain as a function of the oxidation temperature for the same total heating time (about 111 min). The total mass gain increases significantly at temperatures ranging from 1150 to 1190 °C. At 1190 °C, the liquid Fe_2SiO_4 that provides fast diffusion passages promotes the oxidation process, leading to a significant increase in mass gain compared with that at 1150 °C where the Fe_2SiO_4 is a solid phase. The total mass gain increases slowly at temperatures ranging from 1190 to 1235 °C due to the gradual increase in the oxidation rate, as previously mentioned. At temperatures $\geqslant$1235 °C, the total mass gain shows no significant change relative to 1235 °C. At temperatures above 1235 °C, the oxidation rate is higher, as shown in Figure 4b, resulting in a larger total mass gain than that at low temperatures. The mass gains are basically the same at 1235 to 1300 °C because the oxidation rates are similar, indicating that the total mass gain has no relationship with the heating temperatures higher than 1235 °C.

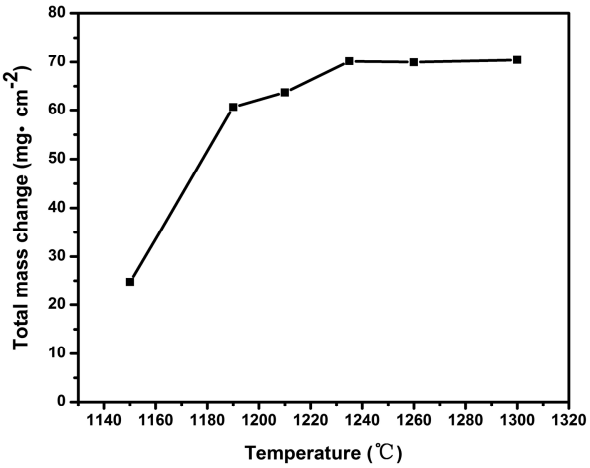

Figure 6. Total mass gain at different oxidation temperatures.

4. Conclusions

The oxidation behavior of silicon-containing steel was studied by using an atmosphere and heating route similar to those applied in the industrial reheating process. The oxidation experiments were carried out on STA at different oxidation temperatures. The effect of oxidation temperature on the oxidation process of silicon-containing steels was investigated. The results show that at temperatures higher than 1235 °C, the mass gain versus time follows a linear law after the intense oxidation temperature (lower than the eutectic temperature of fayalite). The oxidation rate and oxidation total mass gain have no relationship with the heating temperature. However, the oxidation rate first decreases slowly and then drops markedly during the isothermal holding stage at 1190 °C and 1210 °C. With the increase in the heating temperature, the oxidation rate and mass gain increase gradually, and the mass gain with time is close to a parabolic law. Only at the temperatures below 1210 °C does the mass gain versus time follow a parabolic law. Moreover, the penetration depth of Fe_2SiO_4 and the total mass gain increase quickly and then go up slowly before finally becoming basically unchanged at temperatures ranging from 1150 to 1300 °C.

Acknowledgments: The authors gratefully acknowledge the financial supports from National Natural Science Foundation of China (NSFC) (No. 51274154), the National High Technology Research and Development Program of China (No. 2012AA03A504). State Key Laboratory of Development and Application Technology of Automotive Steels (Baosteel Group).

Author Contributions: Guang Xu, supervisor, conceived and designed the experiments; Bei He, conducted experiments, analyzed the data and wrote the paper; Mingxing Zhou, conducted experiments; Qing Yuan, conducted experiments.

Conflicts of Interest: The authors declare no conflict of interest. The founding sponsors had no role in the design of the study; in the collection, analyses, or interpretation of data; in the writing of the manuscript, and in the decision to publish the results.

References

1. Nishimura, T. Rust formation and corrosion performance of Si- and Al-bearing ultrafine grained weathering steel. *Corros. Sci.* **2008**, *50*, 1306–1312. [CrossRef]
2. Hu, H.J.; Xu, G.; Wang, L.; Xue, Z.L.; Zhang, Y.L.; Liu, G.H. The effects of Nb and Mo addition on transformation and properties in low-carbon bainitic steels. *Mater. Des.* **2015**, *84*, 95–99. [CrossRef]
3. Song, L.; Guo, E.; Wang, L.; Liu, D. Effects of silicon on mechanical properties and fracture toughness of heavy-section ductile cast iron. *Metals* **2005**, *5*, 150–161. [CrossRef]
4. Takeda, M.; Onishi, T. Oxidation behavior and scale properties on the Si containing steels. *Mater. Sci. Forum.* **2006**, *522*, 477–488. [CrossRef]

5. Okada, H.; Fukagawa, T.; Ishihara, H. Prevention of red scale formation during hot rolling of steels. *ISIJ Int.* **1995**, *35*, 886–891. [CrossRef]
6. Yuan, Q.; Xu, G.; Zhou, M.X.; He, B. The effect of the Si content on the morphology and amount of Fe_2SiO_4 in low carbon steels. *Metals* **2016**, *6*, 94–103. [CrossRef]
7. Fukagawa, T.; Okada, H.; Maehara, Y. Effect of S in steel on Hydraulic-descaling-ability in Si-added hot-rolled sheets. *ISIJ Int.* **1995**, *81*, 559–564.
8. Fukagawa, T.; Okada, H.; Maehara, Y.; Fujikawa, H. Efeect of small amount of Ni on Hydranlic-decaling-ability in Si-added hot rolled steel sheets. *ISIJ Int.* **1996**, *82*, 63–68.
9. Okada, H.; Fukagawa, T.; Ishihara, H.; Okamoto, A.; Azuma, M.; Matsuda, Y. Effects of hot rolling and descaling condition on red scale defects formation. *ISIJ Int.* **1994**, *80*, 849–854.
10. Suarez, L.; Schneider, J.; Houbaert, Y. High-Temperature oxidation of Fe-Si alloys in the temperature range 900–1250 °C. *Defect. Diffus. Forum.* **2008**, *273–276*, 661–666. [CrossRef]
11. Cao, G.M.; Liu, X.J.; Sun, B.; Liu, Z.Y. Morphology of oxide scale and oxidation kinetics of low carbon steel. *ISIJ Int.* **2014**, *21*, 335–341. [CrossRef]
12. Mouayd, A.A.; Koltsov, A.; Sutter, E.; Tribollet, B. Effect of silicon content in steel and oxidation temperature on scale growth and morphology. *Mater. Chem. Phys.* **2014**, *143*, 996–1004. [CrossRef]
13. Fukagawa, T.; Okada, H.; Maehara, Y. Mechanism of red scale defect formation in Si-Added hot-rolled steel sheets. *ISIJ Int.* **1994**, *34*, 906–911. [CrossRef]
14. Liu, X.J.; Cao, G.M.; He, Y.Q.; Jia, T.; Liu, Z.Y. Effect of temperature on scale morphology of Fe-1.5Si Alloy. *J. Iron Steel Res. Int.* **2013**, *20*, 73–78. [CrossRef]
15. Yang, Y.Y.; Yang, C.H.; Lin, S.N.; Chen, C.H.; Tsai, W.T. Effects of Si and its content on the scale formation on hot-rolled steel strips. *Mater. Chem. Phys.* **2008**, *112*, 566–571. [CrossRef]
16. Staettle, R.W.; Fontana, M.G. *Advances in Corrosion Science and Technology*; Springer-Verlag: New York, NY, USA, 1974; pp. 136–138.
17. Garnaud, G.; Rapp, R.A. Thickness of the oxide layers formed during the oxidation of iron. *Oxid. Met.* **1977**, *11*, 193–198. [CrossRef]
18. Liu, X.J.; Cao, G.M.; Nie, D.M.; Liu, Z.Y. Mechanism of black strips generated on surface of CSP hot-rolled silicon steel. *J. Iron Steel Res. Int.* **2013**, *20*, 54–59. [CrossRef]
19. Atkinson, A. A theoretical analysis of the oxidation of Fe-Si alloys. *Corros. Sci.* **1982**, *22*, 87–102. [CrossRef]
20. Adachi, T.; Meier, G.H. Oxidation of iron-silicon alloys. *Oxid. Met.* **1987**, *27*, 347–366. [CrossRef]
21. Yang, L.; Chien, C.Y.; Derge, G. Self-Diffusion of iron in iron silicate melt. *J. Chem. Phys.* **1959**, *30*, 1627–1630. [CrossRef]
22. Wang, P.W.; Feng, Y.P.; Roth, W.L.; Corbett, J.W. Diffusion behavior of implanted iron in fused silica glass original research article. *J. Non-cryst. Solids* **1988**, *104*, 81–84. [CrossRef]
23. Li, Y.; Fruehan, R.J.; Lucas, J.A.; Belton, G.R. The chemical diffusivity of oxygen in liquid iron oxide and a calcium ferrite. *Metall. Mater. Trans. A* **2000**, *31*, 1059–1068. [CrossRef]
24. Zhang, L.; Zhang, W.; Zhang, J.H.; Li, G.Q. Oxidation kinetics and oxygen capacity of Ti-bearing blast furnace slag under dynamic oxidation conditions. *Metals* **2016**, *6*, 105–120. [CrossRef]
25. Kofstad, P. Low-pressure oxidation of tantalum at 1300–1800 °C. *J. Less Common Metals* **1964**, *7*, 241–266. [CrossRef]
26. Birks, N.; Meier, G.H.; Pettit, F.S. *Introduction to the High-temperature Oxidation of Metals*; Cambridge University Press: Cambridge, UK, 2010; pp. 71–74.
27. Baud, J.; Ferrier, A.; Manenc, J.; Benard, J. The oxidation and decarburizing of Fe-C alloys in air and the influence of relative humidity. *Oxide. Met.* **1975**, *9*, 69–97. [CrossRef]
28. Kofstad, P. On the formation of porosity and microchannels in growing scales. *Oxide. Met.* **1985**, *24*, 265–276. [CrossRef]
29. Kofstad, P.; Hed, A.Z. Defect structure model for wustite. *J. Electrochem. Soc.* **1968**, *115*, 102–104. [CrossRef]